Ship Detection in Ice-Infested Waters Based on Dual-Polarization SAR Imagery

Camilla Brekke, *Member, IEEE*, and Stian Normann Anfinsen, *Student Member, IEEE*

***Abstract*—This letter discusses the potential of automatic ship detection in ice-infested waters based on satellite synthetic aperture radar (SAR) imagery. The popular K-distribution is used to model the backscatter statistics of sea ice clutter. The goodness of fit of this model is assessed with the Kolmogorov–Smirnov and Anderson–Darling test statistics for both VV and VH polarizations. We also test the impact of introducing the Method of Log Cumulant (MoLC) estimator for the shape parameter of the K-distribution. Finally, a constant false-alarm rate ship detection algorithm, applying the K-distribution with the MoLC estimator, is evaluated on dual-polarization RADARSAT-2 SAR data. Our results demonstrate that this is a viable approach to ship detection in ice-infested waters.**

***Index Terms*—Goodness of fit, K-distribution, sea ice, ship detection, synthetic aperture radar (SAR).**

I. Introduction

THERE is rich literature on ship detection in open sea based on satellite-borne synthetic aperture radar (SAR) imagery. Ship detection in ice-infested waters, which is the focus of this letter, has attracted far less attention. As both shipping routes and exploration and production of oil and gas are moving toward higher latitudes, this aspect of marine target detection will be very important to support both environmental and economical interests, as well as health and security.

SAR data are currently used for target detection in operational maritime surveillance services in several countries. The launch of new advanced SAR satellite sensors enables us to use single, dual, and quad polarizations in automatic algorithms for target detection. Target detection in SAR images can be made more reliable if several polarizations are acquired simultaneously at appropriate radar incidence angles. Full polarimetric information is given by the complete complex scattering matrix, and the information about scattering mechanisms of targets can be derived through its various coherent and incoherent decompositions. This can be useful for feature extraction as part of a classification procedure [1].

While quad-polarimetry SAR data have an obvious potential for marine target detection and discrimination of vessels and icebergs in Arctic regions, this data mode is only available for limited swath widths with today's technology. Therefore, when we want to monitor large ocean areas operationally, SAR image products with lower resolution, dual polarization, and wider swaths are currently preferred. Here, we present results based on dual-polarization SAR products, and we focus on the detection stage.

In the literature [2], there are indications that K-distribution is a good model for four-look HH-polarized SAR data from Arctic sea ice. In this letter, we investigate whether this model can also be used for one-look dual-polarization data from VV and VH channels.

In [3], we applied the Method of Log Cumulant (MoLC) as a parameter estimator for the K-distribution. Here, two moment-based parameter estimators, namely, Method of Moments (MoM) and MoLC, are compared based on goodness-of-fit testing of the model with the observed data.

An example from the Barents Sea, with respect to the selection of appropriate polarization and incidence angles, is presented in Section II. The constant false-alarm rate (CFAR) algorithm, the K-distribution, and the parameter estimators evaluated in this study are described in Section III. In Section IV, we discuss the goodness of fit of the K-distribution with the observed data. The experimental results based on three RADARSAT-2 Fine SAR scenes containing ships in ice-infested waters are presented in Section V, and conclusions are given in Section VI.

II. Polarization and Incidence Angles

From an operational point of view, dual-polarization SAR products are interesting due to the possibility of using the same product for both ship and oil pollution detection. However, it is important to select appropriate incidence angles and polarimetric channels for successful ship detection.

We have studied a large fleet of fishing vessels, confirmed by the Norwegian Defence, which was captured by two separate RADARSAT-2 acquisitions. The first scene was acquired with the Wide mode on September 15, 2008 at 06:45 A.M. and the second scene with the ScanSAR narrow mode on the same date at 16:40 P.M. Both acquisitions are four-look SAR images and have an HH and HV combination. The sea surface appears quite homogeneous in both cases.

We have analyzed some of the targets by looking at the peak-to-clutter ratio compared to the incidence angle in both polarization channels. In the Wide-mode scene, the vessels were located at small incidence angles, while in the ScanSAR narrow scene, they were located at larger incidence angles (see Figs. 1 and 2). For the smaller incidence angles of the Wide scene, the targets had a much higher peak-to-clutter ratio in the cross-polarized channel than in the copolarized channel. For the larger incidence angles of the ScanSAR narrow scene, we found a

Manuscript received June 15, 2010; revised August 18, 2010; accepted September 13, 2010.

The authors are with the Department of Physics and Technology, University of Tromsø, N-9037 Tromsø, Norway (e-mail: camilla.brekke@uit.no; stian.normann.anfinsen@uit.no).

Color versions of one or more of the figures in this paper are available online at http://ieeexplore.ieee.org.

Digital Object Identifier 10.1109/LGRS.2010.2078796

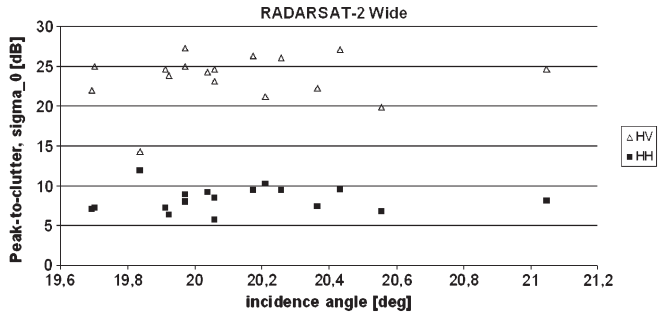

Fig. 1. Peak-to-clutter ratio for a number of vessels in the RADARSAT-2 Wide SGF scene.

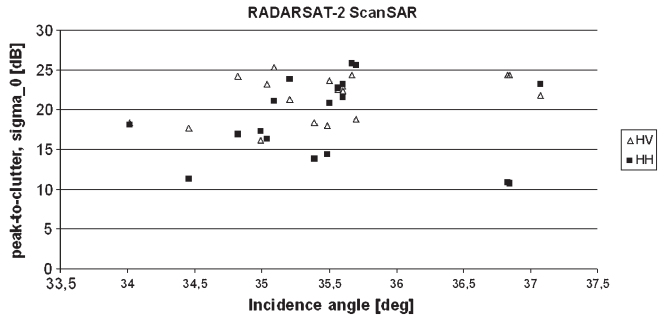

Fig. 2. Peak-to-clutter ratio for a number of vessels in the RADARSAT-2 ScanSAR narrow scene.

much more mixed situation, where both channels could be used for detection as all targets had a peak-to-clutter ratio of more than 10 dB (which is considered an appropriate threshold for SAR data with more than three looks [4]). These findings are in agreement with the experience reported by Kongsberg Satellite Services (KSAT) and European Commission Joint Research Centre [5] and give us an indication that cross-polarization should be preferred for smaller incidence angles.

III. Methodology

The framework of the automatic ship detection algorithm consists of the following elements: 1) land masking to avoid searching for targets on land and to avoid confusing targets with smaller islands; 2) detecting bright targets sequentially in all available channels (HH and HV, or VV and VH); 3) estimating the detection confidence based on the combined results from the various channels; and 4) manual verification. Only step 2) will be addressed here.

A. Bright Target Detection Algorithms

The target is expected to appear as a high intensity outlier in the tail of the histogram of a SAR subimage frame. One of the simplest methods for adaptive thresholding uses a threshold T, which is set to N standard deviations above the mean intensity value $\langle I \rangle$, which is extracted for each frame of size $M \times M$, together with the standard deviation σ:

$$T = \langle I \rangle + N\sigma. \tag{1}$$

More sophisticated CFAR detectors adapt a probability density function (PDF) to the data within a moving subimage frame, and the local threshold is estimated based on the PDF. For a given value of the CFAR, the corresponding local threshold t for each frame is obtained from:

$$CFAR = 1 - \int_0^t P(I)dI \tag{2}$$

with

$$P(I) = \int_0^\infty P(I|z)P(z)dz \tag{3}$$

where $P(I|z)$ is the PDF of the speckle modulated intensity I and $P(z)$ describes the variability of the radar cross section. Equation (3) is based on the product model [6].

B. K-Distribution Model

It is common to model sea clutter with the K-distribution [1], [7]. We shall use it to model sea ice clutter. In the K-distribution, both $P(I|z)$ and $P(z)$ are assumed to be gamma distributed. The resulting intensity PDF will then be given by [6]

$$P(I) = \frac{2}{\Gamma(L)\Gamma(\nu)} \left(\frac{L\nu}{\langle I \rangle}\right)^{\frac{L+\nu}{2}} I^{(L+\nu-2)/2} K_{\nu-L} \times \left[2\left(\frac{\nu L I}{\langle I \rangle}\right)^{1/2}\right] \tag{4}$$

where $K_{\nu-L}$ is a modified Bessel function of the second kind with order $\nu - L$, Γ is the gamma function, L is the number of looks, and ν is an order parameter that defines the shape of the $P(z)$ distribution. It is important to obtain a good estimate for ν to set an appropriate threshold.

1) Parameter Estimators: We have first applied the MoM to estimate the parameters of the K-distribution. Given the intensity moments of the K-distribution [6], the MoM estimate of the order parameter ν is given by

$$\hat{\nu} = \frac{L+1}{L\beta - 1} \tag{5}$$

where $\beta = (\langle I^2 \rangle - \langle I \rangle^2)/\langle I \rangle^2$.

The MoLC is a more advanced method for the estimation of ν [8]. The estimate $\hat{\nu}$ is the solution of the equation

$$\psi_1(\nu) = K_2 - \psi_1(L) \tag{6}$$

where $\psi_1(x) = d^2/dx^2 \log\Gamma(x)$ and $K_2 = (\langle (logI)^2 \rangle - \langle \log I \rangle^2)$ is the second-order sample log cumulant of intensity.

IV. Goodness-of-Fit Testing

In CFAR algorithms for automatic detection of bright targets at sea, the main challenge is to detect the targets appearing on sea surfaces of varying degree of homogeneity and, at the same time, to keep the false-alarm rate down to a predefined level. A commonly used approach is to assume a K-distribution for the intensity, but the K-distribution does not always adequately describe the clutter PDF. Regularly, the actual PDF has an extended tail on the high end side, leading to excess false alarms [7].

TABLE I
AVERAGE $\hat{\nu}$, D_n, AND p VALUES WITH CORRESPONDING VARIANCES FOR DUAL-POLARIZATION RADARSAT-2 SCW EIGHT-LOOK SAR IMAGES. THE VALUES ARE ESTIMATED FROM TEN FRAMES (100 × 100 PIXELS) OF HOMOGENEOUS AND TEN FRAMES OF HETEROGENEOUS SEA SURFACES. THE RESULTS ARE MERGED WITH RESPECT TO CO-POLARIZATION AND CROSS-POLARIZATION DUE TO COMPARABLE ESTIMATES WITHIN THESE CATEGORIES

		MoM	KS test			
	Pol.	$\hat{\nu}$	D_n	$\sigma^2_{D_n}$	p	σ^2_p
Homogemeous sea surface	HH or VV	35	0.01	3e-6	0.63	0.05
	HV or VH	79	0.01	3e-6	0.73	0.06
Heterogeneous sea surface	HH or VV	4	0.06	1e-3	0.00	6e-18
	HV or VH	91	0.01	3e-6	0.66	0.07

TABLE II
AVERAGE $\hat{\nu}$, D_n, A^2, AND p VALUES WITH CORRESPONDING VARIANCES FOR THE DUAL-POLARIZATION RADARSAT-2 FINE SGF ONE-LOOK SAR IMAGES DESCRIBED IN SECTION V-A. THE VALUES ARE ESTIMATED FROM 16 FRAMES (100 × 100 PIXELS) CONTAINING SEA ICE

	MoLC	KS test				AD test			
Pol.	$\hat{\nu}$	D_n	$\sigma^2_{D_n}$	p	σ^2_p	A^2	$\sigma^2_{A^2}$	p	σ^2_p
VV	13	0.01	3e-5	0.49	0.13	1.63	5.57	0.53	0.13
VH	16	0.01	9e-6	0.25	0.06	1.70	1.68	0.31	0.07
	MoM	KS test				AD test			
Pol.	$\hat{\nu}$	D_n	$\sigma^2_{D_n}$	p	σ^2_p	A^2	$\sigma^2_{A^2}$	p	σ^2_p
VV	14	0.06	4e-2	0.55	0.13	1.83	9.68	0.64	0.12
VH	31	0.01	3e-5	0.54	0.11	1.92	14.91	0.57	0.11

Here, both the Kolmogorov–Smirnov (KS) and Anderson–Darling (AD) tests [9] are implemented to evaluate the goodness of fit of the K-distribution on dual-polarization SAR images. The K-distribution is evaluated both on eight-look SAR images containing open sea with various sea states and one-look SAR images containing ice-infested waters. The two parameter estimators, namely, MoM and MoLC, are also compared based on the one-look scenes containing sea ice.

A. KS Test

The KS statistic for a given cumulative distribution function (CDF) $F_0(x)$ is

$$D_n = \sup_x \left| \hat{F}(x) - F_0(x) \right| \tag{7}$$

where $\sup S$ is the supremum of the set S, $\hat{F}$ is the empirical distribution function (EDF), and n is the number of observations. D_n is a measure of the deviation of EDF from $F_0(x)$. The CDF is computed by Monte Carlo simulation of K-distributed variables with the estimated parameters, since the exact CDF is difficult to evaluate numerically.

B. AD Test

To assess if the observations $\{x_1 < \cdots < x_n\}$ come from a distribution with CDF F_0, we can use the AD test, where

$$A^2 = -n - S \tag{8}$$

$$S = \sum_{k=1}^{n} \frac{2k-1}{n} \left[\ln F_0(x_k) + \ln \left(1 - F_0(x_{n+1-k}) \right) \right] \tag{9}$$

where n is the number of observations.

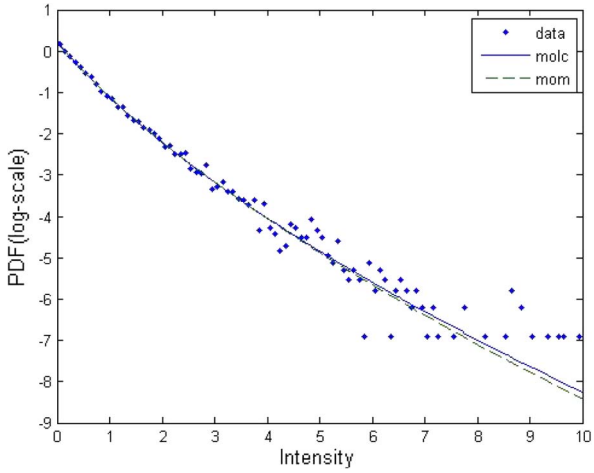

Fig. 3. Histogram based on 100 × 100 observed pixels from ice-infested water. Theoretical K-distributions applying both MoM (KS: $p = 0.39$; AD: $p = 0.55$) and MoLC (KS: $p = 0.99$; AD: $p = 0.95$) are overlaid.

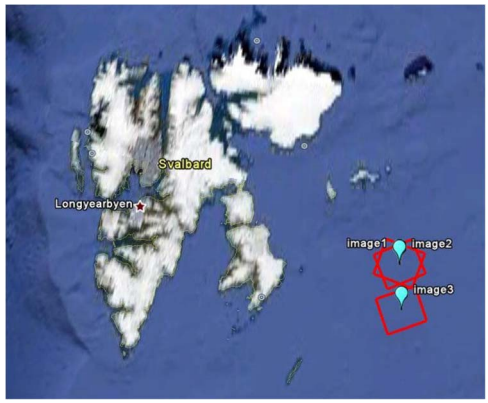

Fig. 4. Study site. Location of SAR scenes indicated.

Fig. 5. (Left) R/V Lance. Length (L): 60.8 m. Breadth (B): 12.6 m. (Right) K/V Svalbard. L: 103.7 m. B: 19.1 m. Photograph by L.-J. Andersson and M. Bengtsson.

TABLE III
ALGORITHM DETECTION RESULTS. CFAR LEVEL APPLIED: 10^-7

Image #	Verified ships	Pol-arization	True alarms	False alarms	Verified ships detected
1	2	VV	2/2	0/2	2
		VH	2/2	0/2	2
2	1	VV	1/1	0/1	1
		VH	1/1	0/1	1
3	1	VV	2/16	14/16	1
		VH	1/1	0/1	1

1) Modeling Sea Clutter: First, the K-distribution is evaluated on eight-look SAR images containing open sea with various sea states. Table I presents the average KS statistic

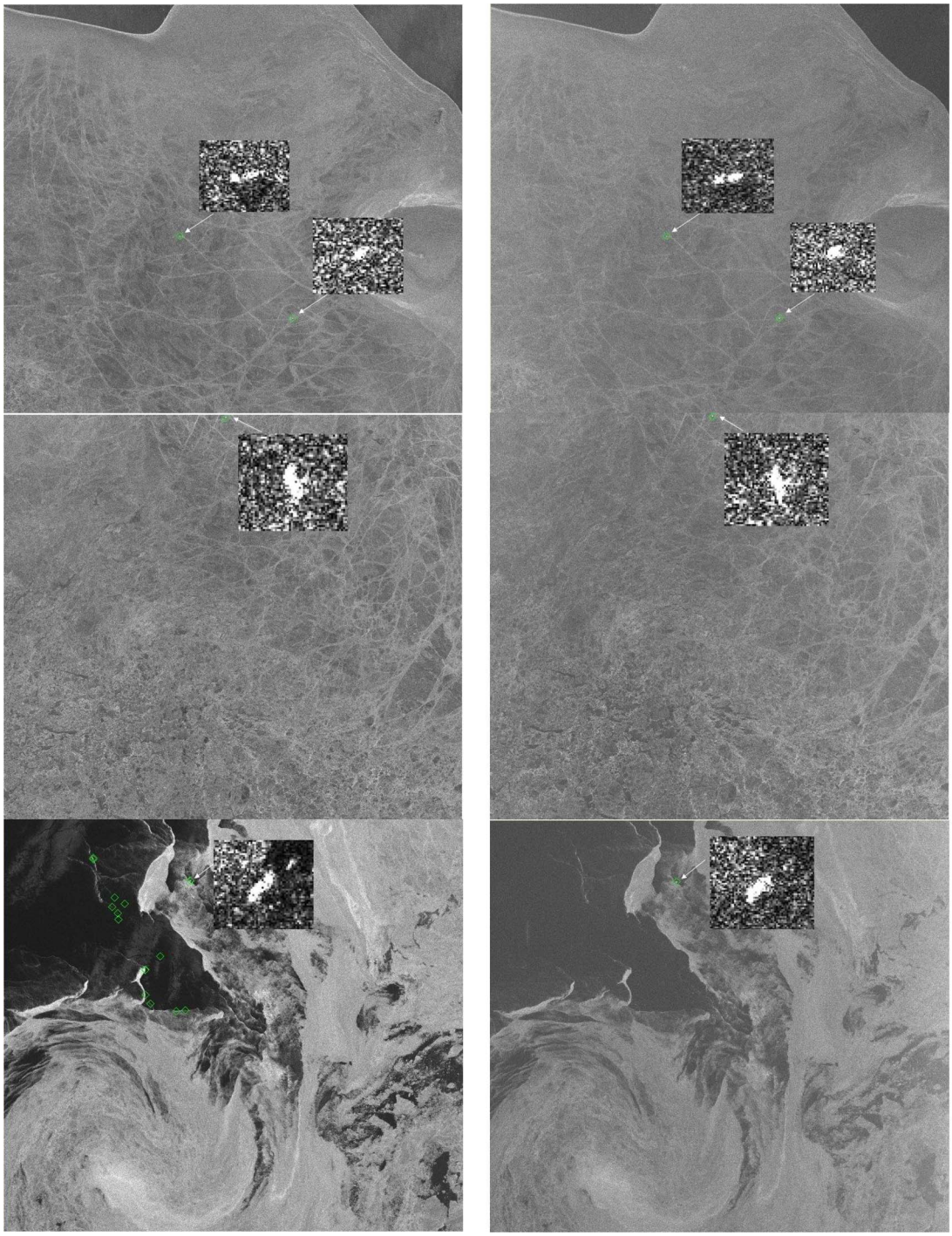

Fig. 6. Detections in images #1–#3. (Left column) VV and (right column) VH channels. CFAR based on the K-distribution with the MoLC as a parameter estimator has been used in all cases. Verified ships pointed out by arrows. (Top row) Image #1. K/V Svalbard to the left and R/V Lance to the right. Both ships detected in both channels. (Middle row) Image #2. R/V Lance detected in both VV and VH. (Bottom row) Image #3. K/V Svalbard located within 20% [10] open ice. The ship is detected in both VV and VH. Copyright raw data MDA, 2009, provided by NSC/KSAT 2010.

D_n and p value with corresponding variances $\sigma^2_{D_n}$ and σ^2_p and order parameter $\hat{\nu}$ estimates. The p value is the probability of obtaining a test statistic whose value is more extreme than the observed one, assuming that our hypothesis is true. In Table I, it is evident from the very low p value of the copolarized heterogeneous cases that the K-distribution hypothesis should be rejected. The average p values, ranging from 0.63 to 0.73, for the remaining cases in Table I support the selection of the K-distribution as a statistical model.

High values for $\hat{\nu}$ indicate that the intensity tends to a gamma distribution. The results for $\hat{\nu}$ in Table I therefore tell us that the cross-polarization measurements tend more toward a gamma distribution than the co-polarization measurements.

2) Modeling Sea Ice: Second, the K-distribution is evaluated as a model for ice-infested scenes. Here, we have also applied the AD test, which gives more weight to the tail than the KS test. Table II presents the results based on a number of manually selected seemingly homogeneous samples from

the three images described in Section V-A. The average p values, ranging from 0.25 to 0.64, support the selection of the K-distribution as a statistical model for the homogeneous regions in the ice-infested one-look scenes. The results are slightly better for VV than VH, as can be seen from the higher p values. Fig. 3 shows the histogram for the observed data and the theoretical K-distributions for one particular frame in the VV channel containing sea ice, showing that this frame is at least nearly K-distributed.

3) Estimator Comparison: Third, the MoM and MoLC estimators are compared. These results are also presented in Table II. Studying the test statistics D_n and A^2, we observe that the MoLC yields equal or lower (i.e., better fit) average values than the MoM for both VV and VH. The MoLC estimator has the lowest variance, as can be seen from the $\sigma^2_{D_n}$ and $\sigma^2_{A^2}$ values. However, if we study the average p values, we can see from Table II that the MoM yields better (higher) p values than the MoLC. However, the variance σ^2_p of the MoLC is equal or lower in three out of the four cases studied. In summary, the experimental results indicate that the MoLC produces estimates with lower variance than the MoM. No significant difference between the two estimators was however found based on the KS and AD tests. Note that only 32 frames, namely, 16 VV and 16 VH, of size 100 $\times$ 100 pixels are studied here.

V. Experimental Results

The adaptive CFAR algorithm described is evaluated on RADARSAT-2 SAR imagery containing sea ice and ships. In this letter, a moving subimage frame of size 100 $\times$ 100 pixels is applied. The MoLC has been applied to parameter estimation for all three images studied. Scenes with homogeneous sea ice, apparently free from structures such as cracks and ridges, and scenes covering the ice edge, open water, and a mixture of open water and ice-infested water are evaluated.

A. Data Set and Study Site

The data set consists of three RADARSAT-2 dual-polarization, i.e., VV and VH, Fine-mode SAR Georeferenced Fine (SGF) images acquired outside the coast of Svalbard in May 2009 (see Fig. 4). Image #1 is acquired in May 16 at 05:16 UTC at descending orbit, beam type F22, and incidence angles in the range from 33.3° to 36.4°. Images #2 and #3 are acquired at ascending orbit, in May 17 at 14:44 UTC and May 20 at 14:57 UTC, beam types F21 and F1, and incidence angles in the range from 34.8° to 37.9° and from 37.7° to 40.7°, respectively. All three images contain verified ships, specifically repeated acquisitions of K/V Svalbard and R/V Lance, located in ice-infested water [10] (see Fig. 5).

B. Performance Evaluation

Table III presents the detection results. Based on an initial pixel-based detection (binary classification), target pixels are merged into clusters based on an eight-neighbor search. The target cluster positions have been compared with the *in situ* information given by Babiker *et al.* [10]. In Fig. 6, the detection results of the three SAR scenes are overlaid. All potential targets found by the algorithm are indicated by the colored squares. All ships in all images are detected by the algorithm. Two adjacent target clusters, and thus two alarms, are generated by the same ship (2 out of 16 alarms) in image #3. However, 14 out of 16 alarms in the mixed open sea and ice situation in the VV channel of image #3 are false alarms. In this case, this can be explained by a higher contrast between ice and water in co-polarization compared to cross-polarization.

VI. Conclusion

This letter has shown the potential of automatic ship detection in ice-infested waters based on satellite SAR images. Applying goodness-of-fit tests, we have demonstrated that the K-distribution is a suitable statistical model for sea ice in one-look intensity images of VV and VH polarizations. The MoLC is shown to produce estimates with lower variance than the MoM, as expected from theoretical comparisons. The performance of a CFAR algorithm based on the K-distribution, utilizing the MoLC, also shows promising results for scenes of smooth ice, both VV and VH, but produces some false alarms in mixed sea ice and open water situations in the VV channel.

References

[1] R. B. Olsen , Analysis of Options for MARISS Services Extension, GMES Services Element Consolidation for Maritime Security, MARISS-FFI-TN2-TN-015, 2009.

[2] I. R. Joughin, D. B. Percival, and D. P. Winebrenner, "Maximum likelihood estimation of K distribution parameters for SAR data," *IEEE Trans. Geosci. Remote Sens.*, vol. 31, no. 5, pp. 989–999, Sep. 1993.

[3] C. Brekke, S. N. Anfinsen, and T. Eltoft, "Marine target detection based on dual channel SAR images," in *Proc. EUSAR*, Aachen, Germany, 2010, pp. 786–789.

[4] T. Arnesen and R. B. Olsen, "Literature review on vessel detection," Forsvarets Forskningsinstitutt, Kjeller, Norway, FFI-Rapport-2004/02619, 2004.

[5] M. Indregard, T. Bauna, H. Van Wimersma Greidanus, and J. Cicuendez-Perez, "Dual polarisation SAR for combined vessel and oil spill detection," in *Proc. 33rd ISRSE*, Stressa, Italy, 2009, pp. 813–816.

[6] C. Oliver and S. Quegan, *Understanding Synthetic Aperture Radar Images*. Raleigh, NC: SciTech Publishing, 2004.

[7] H. Greidanus, "Satellite imaging for maritime surveillance of the European seas," in *Remote Sensing of the European Seas*. New York: Springer-Verlag, 2008, pp. 343–358.

[8] J.-M. Nicolas, "Introduction aux Statistiques de Deuxième Espèce: Applications des log-moments et des log-cumulants á l'analyse des lois d'images radar," *Trait. Signal*, vol. 19, no. 3, pp. 139–167, 2002.

[9] R. B. D'Agostino and M. A. Stephens, *Goodness-of-Fit Techniques*, vol. 68. New York: Marcel Dekker, 1986, ser. Statistics, textbooks and monographs.

[10] M. Babiker, K. Kloster, S. Sandven, and R. Hall, "The utilisation of satellite images for the oil in ice experiment in the barents sea in May 2009," NERSC, Berkeley, CA, Tech. Rep. 305, Dec. 22, 2009.